Environmental and
Biogeochemical Processes

https://doi.org/10.48130/ebp-0026-0017

Original Research

Open Access

Effects of O_2 on coupled structural transformation of birnessite and degradation of humic substances

Peng Yang[1,2#], Qian Wang[1,3#] and Mengqiang Zhu[1,4*]

Received: 5 June 2026

Revised: 25 August 2026

Accepted: 24 September 2026

Published online: 2 November 2026

Abstract

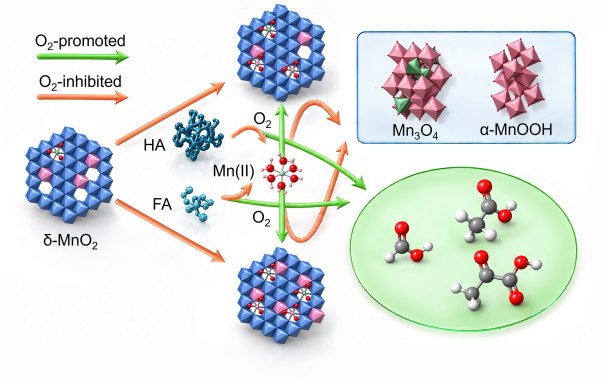
Manganese (Mn) oxides are reactive redox interfaces that can couple Mn cycling with the transformation of humic substances (HS). During these reactions, HS can reduce Mn oxides, while Mn oxides can oxidize and transform organic compounds. These reactions occur across environments with variable O_2 availability, but the role of O_2 in controlling coupled Mn-organic matter transformations remains unclear. Here, we investigated how a nanoparticulate layered Mn oxide (δ-MnO_2) reacts with different types of humic substances (fuvic versus humic acid) under varying environmental conditions. The results show that O_2 is a key factor controlling Mn oxide transformation pathways and the fate of reduced Mn. Specifically, O_2 shifts reaction pathways from secondary mineral formation toward Mn incorporation into layers, and promotes organic matter oxidation, ascribed to O_2 interactions with HS and dissolved Mn. The extent and nature of these effects depend strongly on the type of humic substance and the degree of reducing conditions. Overall, these findings show that O_2 actively regulates Mn oxide–HS reactions by altering the partitioning of reduced Mn among dissolved, structural, vacancy-associated, and secondary mineral phases, with reaction pathways strongly controlled by the type and loading of humic substances.

Keywords: Manganese oxides, Redox, Mineral transformation, Organic matter degradation, Humic substances, Humic acid, Fulvic acid

Highlights

- Oxygen (O_2) regulates coupled Mn oxide–humic substance redox reactions by controlling Mn transformation pathways.
- Oxygen shifts reduced Mn from secondary mineral formation toward structurally incorporated Mn species.
- Humic substance type and reductant loading govern the extent of O_2-driven Mn oxide and organic matter transformations.

Graphical abstract



# Authors contributed equally: Peng Yang and Qian Wang

* Correspondence: Mengqiang Zhu (mqzhu@umd.edu)

Full list of author information is available at the end of the article.

https://doi.org/10.48130/ebp-0026-0017

Introduction

Birnessite is the most abundant and reactive manganese (Mn) oxide mineral in nature, affecting elemental cycling due to its exceptional sorption and oxidation capabilities[1–7]. The properties and reactivity of birnessite are primarily governed by Mn cation vacancies and Mn oxidation states, particularly the concentration and spatial arrangement of Mn(III) within its structure[6–11]. Partial reductive dissolution of birnessite can strongly modify its structural and chemical characteristics and may even induce transformation to other Mn oxide phases[7,9,12]. Such reduction can occur across a range of pH conditions, reductant-to-birnessite ratios, and in the presence of coexisting cations and anions[4,7,9,12,13].

Dissolved organic matter (DOM) is a ubiquitous and abundant reductant in soils and aquatic systems, including water columns, sediments, and porewaters. Redox reactions between DOM and Mn oxides influence not only Mn biogeochemical cycling but also DOM transformation, persistence, and reactivity[9,12–25]. On one hand, oxidation of DOM by Mn oxides can lead to degradation into high-molecular-weight segments, low-molecular-weight organic compounds, carbon monoxide, and CO_2, promoting decomposition[9,12–15,20,26–28]. These reactions contribute to litter decomposition processes, which have been shown to correlate strongly with Mn concentrations in plant litter[29–32], although dissolved Mn(III) species may play a more dominant role. On the other hand, Mn oxides can promote oxidative polymerization of DOM components, including polyphenols and sugars, forming larger and more complex molecules, increasing the stability of organic matter[15,16,18,28,33,34].

Because DOM is chemically heterogeneous, studies of specific DOM fractions are needed to resolve the mechanisms governing its interactions with Mn oxides. Humic substances (HS), including humic acid, fulvic acid, and humin, constitute an important fraction of DOM[35] and are widely used as representative substrates for investigating these interactions. For example, biogenic Mn oxides exhibit higher reactivity toward organic carbon than ferromanganese cave deposits[36]. DOM–MnO_2 interactions release uranium through coupled DOM oxidation and MnO_2 reduction[37]. MnO_2 oxidizes DOM to oxygen-depleting and aliphatic compounds[38], while coexisting cations inhibit phenol oxidation[39]. DOM reactions with Mn oxides also form carbon-Mn oxide colloids, whose stability depends on metal cations, with Mn(II) providing the greatest stabilization[40]. Moreover, δ-MnO_2, a nano-particulate birnessie phase, promotes the humification of fulvic acid (FA), but not humic acid (HA)[41,42], likely through polymerization, with high-molecular-weight FA showing stronger adsorption and reducing capacity toward MnO_2[43]. Our previous studies demonstrated that adsorption and oxidation of FA, a HS surrogate, by birnessite under anoxic conditions increased Mn(III) and Mn(II) concentrations in the birnessite structure or induced its transformation into hausmannite (Mn_3O_4) and MnOOH phases, depending on pH, FA/birnessite mass ratios, the type and concentration of coexisting cations, and reaction time[9,12]. Specifically, the δ-MnO_2 structure became progressively enriched in both Mn(II) and Mn(III) at pH 8, but only Mn(II) at pH 4 and 6[12]. These findings contrast with other studies using X-ray photoelectron spectroscopy (XPS), which reported that solids contained 26%–56% Mn(III) after birnessite reacted with humate and low-molecular-weight organics (e.g., oxalate, triclosan, aniline, and phenol) at pH ~5 under oxic conditions[44–47]. In addition, a large portion of FA molecules were involved in degradation by Mn oxides under aerobic conditions, particularly polycyclic aromatic hydrocarbons, polyphenols, highly unsaturated and phenolic compounds, with more thorough degradation at pH 4 than at pH 6, whereas polymerization was not observed[48].

The reactions between Mn oxides and HS often occur in environments with variable levels of O_2. However, as far as the authors know, there have been a very limited number of studies examining the effect of O_2 on the coupled transformation of Mn oxides and HS. A recent study by Zou et al.[49] showed that O_2 plays a key role in the humification of catechin and glycine to form HA and FA, and MnO_2 and O_2 synergistically enhance the formation of HA. In contrast, another study showed that O_2 inhibits FA oxidation by δ-MnO_2[50]. The observed high Mn(III) fractions in those Mn oxide–OM studies[44–47] may result from oxidation of adsorbed Mn(II) by O_2 on birnessite surfaces or the formation of low-valence Mn oxide (LVMO) phases. Mn(III) incorporation into birnessite can occur via oxidation of adsorbed Mn(II) by atmospheric O_2 at pH ≥ 7[51], whereas Mn(II) oxidation by O_2 is negligible at pH < 6[52]. Similarly, studies by Mandernack et al.[53] and Tu et al.[54] showed that birnessite–Mn(II) interactions under oxic conditions produce various Mn(III)-containing phases, including feitknechtite (β-MnOOH), groutite (α-MnOOH), manganite (γ-MnOOH), and hausmannite at pH ≥ 6, which is attributed to surface-catalyzed Mn(II) oxidation by O_2. However, some Mn(II,III) oxides, such as hausmannite, are unstable in alkaline media in the presence of O_2, converting to birnessite[55] or manganite[56].

To examine how O_2 affects the birnessite–HS reactions, we conducted batch experiments by reacting δ-MnO_2 with HA or FA at pH 5 or 8 and HS/solid mass ratios of 0.1 or 1 in the presence or absence of atmospheric O_2. HA and FA serve as HS surrogates and differ in chemical characteristics such as molecular weight and the abundance of carboxyl and phenolic OH groups[57–59]. HA extracted from soils is generally less acidic and contains fewer reducing functional groups (e.g., phenols and hydroquinones) than FA isolated from surface waters[60], likely resulting in lower reducing capacity for HA.

Materials and methods

Materials

δ-MnO_2 was synthesized by reducing $KMnO_4$ with $Mn(NO_3)_2$ under basic conditions, following the procedure described in Wang et al.[12] Humic acid used in this study was extracted from soils collected at the Main Agricultural Experiment Station of the University of Arkansas (Fayetteville, AR, USA) using the method of He et al.[61], and subsequently purified according to the International Humic Substances Society protocol[62]. The HA material was used in our previous study[13]. Suwannee River fulvic acid was obtained from the International Humic Substances Society. All inorganic chemicals were of analytical grade.

Reaction of HS with δ-MnO_2

The experiments were conducted in 500 mL capped polyethylene bottles containing 50 mmol/L NaCl to maintain background ionic strength under ambient air conditions or inside a COY vinyl anaerobic chamber (95% N_2 + 5% H_2) equipped with a Pd catalyst. HA or FA (0.3 g/L) was reacted with δ-MnO_2 (3 or 0.3 g/L) in batch systems at pH 5 or 8 for up to 600 h, resulting in HS-to-solid mass ratios (R) of 0.1 or 1. The experimental procedures followed those described in our previous study[12]. At selected time intervals, 20 mL aliquots of the suspensions were withdrawn and filtered through 0.22 μm nitrocellulose

membranes. Filtrates were analyzed for dissolved Mn ($[Mn]_{dis}$) using inductively coupled plasma-optical emission spectrometry (ICP-OES), which had a detection limit of 0.1 μg/L (0.002 μmol/L). However, reported values were kept at 0.1 μmol/L precision for clarity. The retention of Mn(II) on nitrocellulose was expected to be negligible based on a previous study[63]; however, the concentration of Mn(III)-ligand complexes might be underestimated due to their stronger retention by the membranes[64]. Therefore, $[Mn]_{dis}$ should reflect more Mn(II) than dissolved Mn(III)-ligand species. The recovered solids were air-dried and ground before further characterization with synchrotron X-ray techniques.

Characterization of reacted solids

Both XRD and total X-ray scattering data for pair distribution function (PDF) analysis were collected from the air-dried solids using a 58.6772 keV X-ray (λ = 0.2113 Å) at beamline 11-ID-B of the Advanced Photon Source (APS), Argonne National Laboratory. The sample-to-detector distances were approximately 100 cm for XRD and 15 cm for total scattering PDF. Data collection and processing followed the procedures described in Wang et al.[12]. Briefly, two-dimensional XRD and PDF scattering images were integrated into one-dimensional scattering intensity vs scattering vector (Q) using *FIT2D*[65]. The integrated XRD data were directly used for phase identification after subtracting empty Kapton tubing for background correction. To obtain the PDF, the integrated one-dimensional total scattering data were converted into the reduced total structure function $F(Q)$ using *PDFgetX2*[66], where $F(Q) = Q[S(Q) - 1]$ and $S(Q)$ is the structure function. Finally, the PDF, $G(r)$, was obtained by Fourier transform of $F(Q)$ through $G(r) = \frac{2}{\pi}\int_{Q_{min}}^{Q_{max}} F(Q)\sin(Qr)\,dQ$[67] using *PDFgetX2*.

To estimate the content of Mn(II), Mn(III), and Mn(IV) in the reacted solids, selected samples were subjected to Mn K-edge X-ray absorption near-edge structure (XANES) spectroscopy and subsequent linear combination fitting (LCF) analysis. The LCF analysis was conducted over −20 and +30 eV of E_0 in the derivative-normalized absorption coefficient (μ) using *ATHENA*[68] with standards including hureaulite [Mn(II)], pyroxmangite [Mn(II)], tephroite [Mn(II)], Mn_2O_3 [Mn(III)], groutite [Mn(III)], feitknechtite [Mn(III)], manganite [Mn(III)], pyrolusite [Mn(IV)], ramsdellite [Mn(IV)], KBi [Mn(IV)], $Ca_2Mn_3O_8$ [Mn(IV)], and TcBi [Mn(III,IV)] from Manceau et al.[69]. Energy was not allowed to shift during the LCF analysis.

Characterization of reacted HA and FA

For the reacted HA and FA, the E_2/E_3 ratio (absorbance at 250 nm divided by that at 365 nm) was determined from the filtrate UV-vis spectra and used to assess compositional changes in the HA and FA.

In addition, concentrations of low-molecular-weight (LMW) organic molecules of HS oxidation, including acetate, formate, and pyruvate, were measured by ion chromatography (IC) equipped with a conductivity detector. Formate and pyruvate could not be differentiated; therefore, their concentrations were reported as combined values. Our previous work provides details for the IC measurement[13].

Results

Dissolved Mn

The release kinetics of dissolved Mn during HS-driven reduction of δ-MnO_2 were influenced by R, HS type (HA vs FA), pH, and redox conditions (oxic vs anoxic). In the R = 0 experiments (i.e., in the absence of reductants), no dissolved Mn was detected (data not shown). At R = 0.1 and 1, $[Mn]_{dis}$ generally increased with time under anoxic conditions in HA-amended systems (Fig. 1a, b). For a given R, lower pH (pH 5 vs pH 8) resulted in higher $[Mn]_{dis}$, indicating that MnO_2 reduction is more favorable at lower pH. At pH 8, $[Mn]_{dis}$ was higher at R = 1 than at R = 0.1 (Fig. 1b), reflecting the greater availability of HA to reduce δ-MnO_2. In contrast, at pH 5, the HA system with R = 0.1 yielded higher $[Mn]_{dis}$ at later reaction stages (Fig. 1a), attributable to the higher solid concentration used in the R = 0.1 experiments. Compared with anoxic systems, oxic conditions generally produced slightly lower $[Mn]_{dis}$ (Fig. 1a, b), with the difference becoming much more pronounced at pH 8 (Fig. 1b). Notably, at pH 8 and R = 1, $[Mn]_{dis}$ under oxic conditions increased initially but reached a plateau of 7.8 μmol/L after approximately 120 h, whereas under anoxic conditions $[Mn]_{dis}$ continued to increase throughout the experimental period, reaching 64.2 μmol/L by the end of the experiment (Fig. 1b).

In the FA systems, a similar trend was observed (Fig. 1c). At R = 1 under anoxic conditions, $[Mn]_{dis}$ increased continuously to 185.4 μmol/L by the end of the experiment, whereas under oxic conditions it increased to 9.9 μmol/L and subsequently decreased to 2.7 μmol/L. The higher $[Mn]_{dis}$ indicates that FA exhibited stronger reductive reactivity toward δ-MnO_2 than HA. At R = 0.1, negligible dissolved Mn was detected.

HS removal and degradation

Adsorption onto solid particles was the primary pathway for HS removal, as indicated by the UV-vis spectra of the remaining HS during δ-MnO_2 reduction (Supplementary Fig. S1a–S1h). Under anoxic conditions, the UV-vis absorbance of the remaining HA in the filtrates decreased across all wavelengths with increasing reaction time, indicating that HA removal was dominated by adsorption onto the solids[9,12,18]. The E_2/E_3 ratio, which is inversely correlated with the aromaticity of HA[70,71], generally increased over time (Fig. 2a, b). This increase indicates preferential removal of the more aromatic and higher-molecular-weight fractions of HA through adsorption and/or oxidation[9,12]. This pattern was more pronounced at lower R and lower pH (Fig. 2a, b). Compared with anoxic systems, E_2/E_3 values were slightly higher under oxic conditions regardless of R and pH (Fig. 2a, b), reflecting modestly stronger adsorption and/or oxidation in the presence of O_2.

HA was oxidized to LMW organic molecules by δ-MnO_2 and/or O_2 (Fig. 3a–d). However, no clear increase or decrease trend in LMW organic molecule concentrations was observed, suggesting that production and consumption processes occurred simultaneously. The production of LMW organic molecules was enhanced under oxic conditions for HA at pH 5, whereas the effect was not obvious or was even opposite at pH 8.

Compared with HA, FA showed similar patterns (Figs 2c, d, 3e, f; Supplementary Fig. S1i–S1l). The E_2/E_3 ratios of residual FA were greater than those of HA at pH 8, suggesting stronger oxidation. Another notable feature is that the enhancement of oxidation by oxygen was more pronounced for FA (Fig. 2c, d), as reflected by the larger differences in E_2/E_3 values between anoxic and oxic conditions and the much higher concentrations of LMW organic molecules under oxic conditions for most time points. Lastly, concentrations of LMW organic molecules were highest within the first 30 min and decreased sharply by 1 h, indicating rapid consumption after the initial production phase.

Structural alterations of δ-MnO_2

The PDF analysis was used to evaluate the local structural evolution of δ-MnO_2 during reactions with HS (Supplementary Fig. S2). As the

https://doi.org/10.48130/ebp-0026-0017

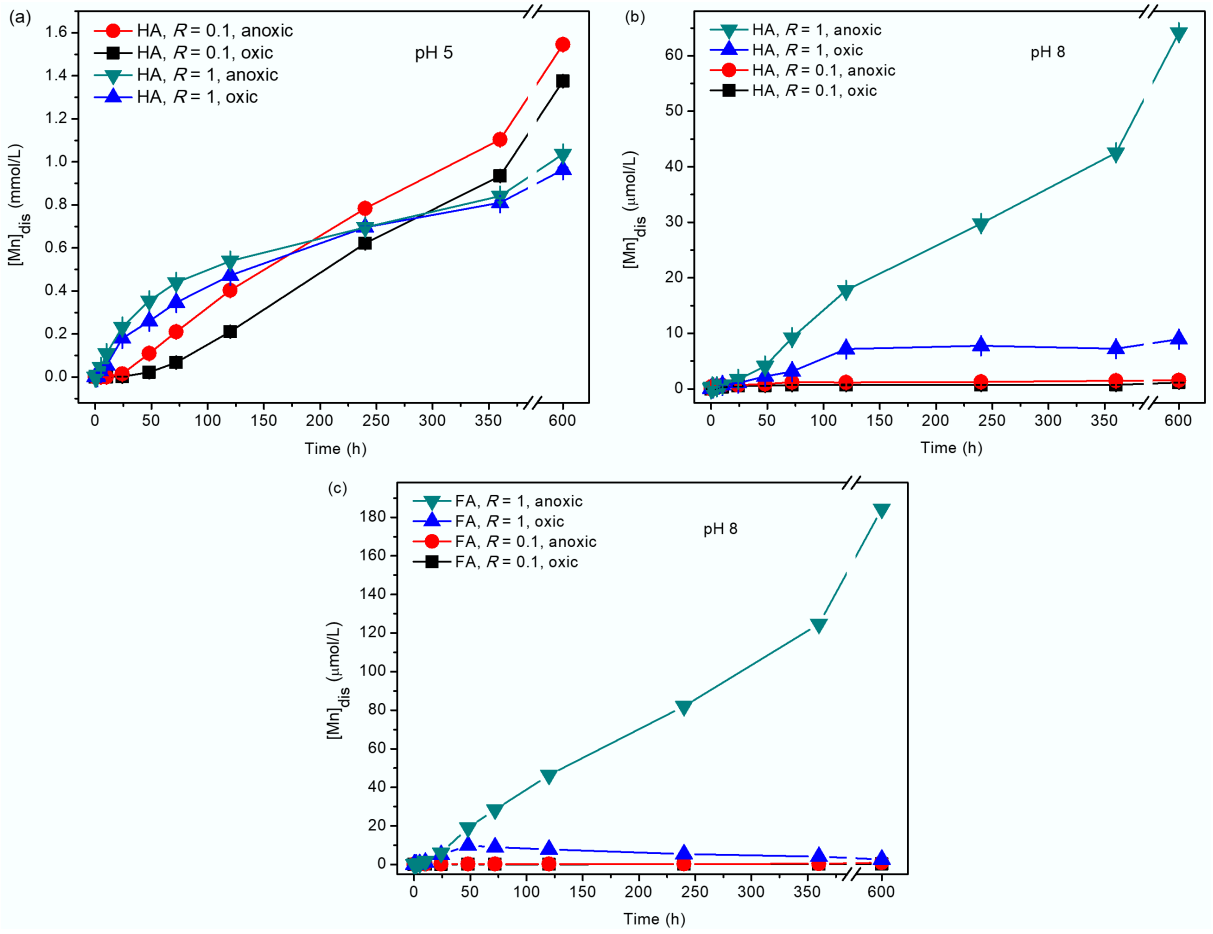


Fig. 1 Dissolved Mn concentration ($[Mn]_{dis}$) during the reduction of δ-MnO_2 by HA at (**a**) pH 5, (**b**) pH 8, and (**c**) FA at pH 8 with R = 0.1 and 1 under anoxic or oxic conditions. The errors resulted from repeated concentration measurements using ICP-OES.

reaction progressed, both Mn–Mn interatomic distances and correlation abundances changed. In particular, the Mn–Mn edge-sharing pairs within the layers (Mn_L–Mn_L) at ~2.9 Å and the second-nearest Mn–Mn corner-sharing pairs associated with vacancies (Mn_L–Mn_{IL}) at ~5.3 Å exhibited shifts in peak position and/or changes in peak intensity as the structural composition evolved over time (Supplementary Fig. S2). Specifically, the Mn_L–Mn_L distance shifts to larger r values with increasing Mn(III) content in the layers, whereas the Mn_L–Mn_{IL} peak area increases as more Mn(II,III) adsorb at vacancy sites[9].

These changes were quantified by tracking the Mn_L–Mn_L peak position and Mn_L–Mn_{IL} peak area as functions of time (Fig. 4). In HA systems at pH 5 and R = 0.1, the Mn_L–Mn_L distance decreased rapidly within the first 24 h and then decreased slightly thereafter under both oxic and anoxic conditions (Fig. 4a). The abundance of Mn_L–Mn_{IL} pairs increased and approached a plateau near 72 h (Fig. 4b). At R = 1, similar but smaller changes were observed (Fig. 4a, b).

At pH 8 and R = 0.1, the Mn_L–Mn_L distance decreased slightly over 600 h under anoxic conditions but increased slightly under oxic conditions (Fig. 4c). Meanwhile, Mn_L–Mn_{IL} abundance increased steadily under both conditions (Fig. 4d). In contrast, at R = 1 the Mn_L–Mn_L distance generally decreased over time under both oxic and anoxic conditions, although some fluctuations were observed (Fig. 4c). The Mn_L–Mn_{IL} abundance increased under both conditions, with larger increases under anoxic conditions. Moreover, the extent of Mn_L–Mn_{IL} growth was greater at R = 1 than at R = 0.1 (Fig. 4d).

In FA systems at pH 8, both the Mn_L–Mn_L distance and Mn_L–Mn_{IL} abundance increased in all systems, with larger changes at R = 1 (Fig. 4e, f). The Mn_L–Mn_L distance was longer while Mn_L–Mn_{IL} abundance was smaller under oxic conditions, indicating greater Mn(III) incorporation in the layers but less Mn(II,III) adsorption at vacancy sites[9].

The XRD patterns of δ-MnO_2 reacted with HS also provide evidence of subtle structural changes. In HA systems, the (002) reflection (d = 3.6 Å) progressively weakened with increasing reaction time (Fig. 5; Supplementary Fig. S3), indicating fewer stacked MnO_6 layers and/or a reduced degree of layer parallelism[12,72]. In addition, a pronounced dip at ~2 Å developed in most cases, resulting from increasing numbers of vacancies capped by Mn(II,III)[9,12,73,74]. The presence of O_2 inhibited both the decrease of the (002) reflection and the development of the dip. The evolution of this dip is consistent with the increase in the PDF peak area at r ≈ 5.3 Å described above. In FA systems, the weakening of the (002) reflection and the development of the dip were even more pronounced (Fig. 6).

Mineral phases

The mineral transformations of reacted δ-MnO_2 were characterized by XRD (Figs 5, 6; Supplementary Fig. S3). Hausmannite formed in all HA

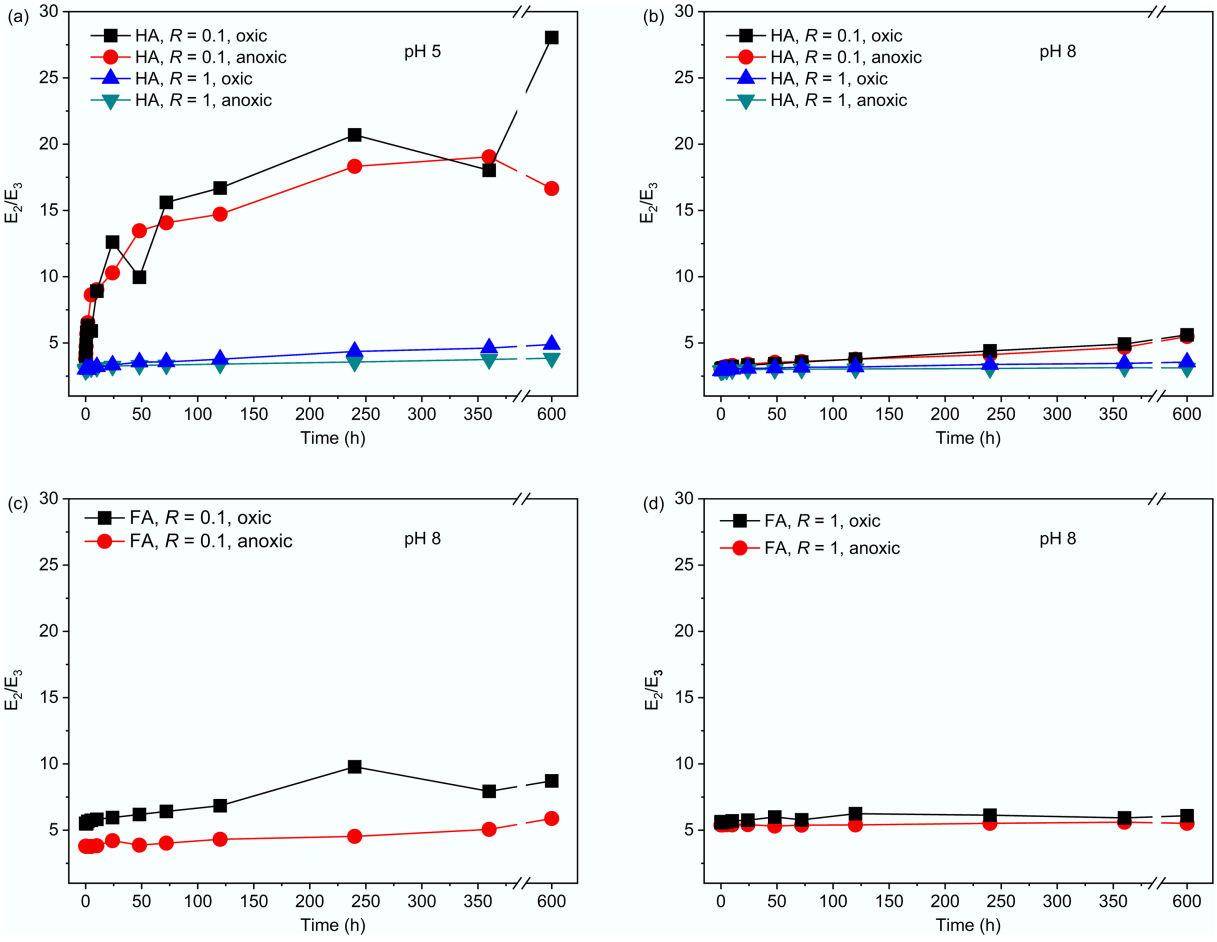


Fig. 2 E_2/E_3 of HA remained in the reactions with δ-MnO_2 at (**a**) pH 5 and (**b**) pH 8 with R = 0.1 and 1 and FA remained at pH 8 with (**c**) R = 0.1 and (**d**) R = 1. Data for FA under anoxic conditions were adopted from Wang et al.[12].

systems, and its abundance increased with time (Fig. 5; Supplementary Fig. S3). Higher pH, lower R, or O_2 suppressed the formation of hausmannite, as shown by the decreased intensity of the hausmannite reflection peak. At R = 1 under oxic or anoxic conditions, groutite appeared as early as 0.02 h (Fig. 5). However, groutite remained low in abundance and showed little or no change over time compared with hausmannite (Fig. 5). In FA systems, hausmannite only formed at R = 1 (Fig. 6c, d), and the presence of O_2 suppressed its formation.

Mn oxidation states in solids

The variations in Mn(II) and Mn(III) content in the solids, estimated by Mn XANES LCF analysis (Supplementary Fig. S4), differ between HA and FA systems. In the HA systems, Mn(III) content in the solids generally decreased, whereas Mn(II) content increased or remained relatively unchanged with reaction time (Fig. 7a–d). These variations are consistent with the decreasing Mn_L–Mn_L distance and the increasing abundance of Mn_L–Mn_{IL} atomic pairs observed in the PDF analysis above, indicating that most Mn(III) resides within the layers while most Mn(II) is adsorbed at vacancy sites. The presence of O_2 seemed to inhibit Mn(III) production while showing little alteration in Mn(II) content except for the HA system at pH 5 and R = 1, where O_2 enhanced Mn(II) production.

In the FA systems at R = 0.1 and 1 under anoxic conditions, both Mn(III) and Mn(II) increased over time (Fig. 7e, f), consistent with our previous study[12] and the PDF results discussed above. However, under oxic conditions, Mn(III) increased at R = 0.1 but slightly decreased at R = 1 over time, while Mn(II) showed little change at R = 0.1 but increased at R = 1. These variations do not align with the atomic distances and pair abundances observed in the PDF analysis, probably because of the interactions of Mn(III) with LMW organic acids (see discussion below). Another notable observation is that, except at pH 8 with R = 1, the Mn(II) and Mn(III) contents were lower than those in the HA systems. For both HA and FA systems, the starting material δ-MnO_2 had about 10% Mn(II) and 16% Mn(III), which changed significantly at the beginning of the reactions, indicating a rapid compositional change during the interactions with HS.

Discussion

The effects of O_2 were manifested by decreased $[Mn]_{dis}$ (Fig. 1), inhibited solid Mn(III) production, enhanced Mn(III) accumulation within the layers (Fig. 4), suppressed formation of hausmannite and groutite (Figs 5, 6; Supplementary Fig. S3), and improved degradation of HS (Figs 2, 3; Supplementary Fig. S1). The following sections discuss each of these effects in detail.

Decreased $[Mn]_{dis}$

The decrease in $[Mn]_{dis}$ may result from inhibited Mn(II) production and/or enhanced consumption of dissolved Mn by O_2. First, O_2 could

https://doi.org/10.48130/ebp-0026-0017

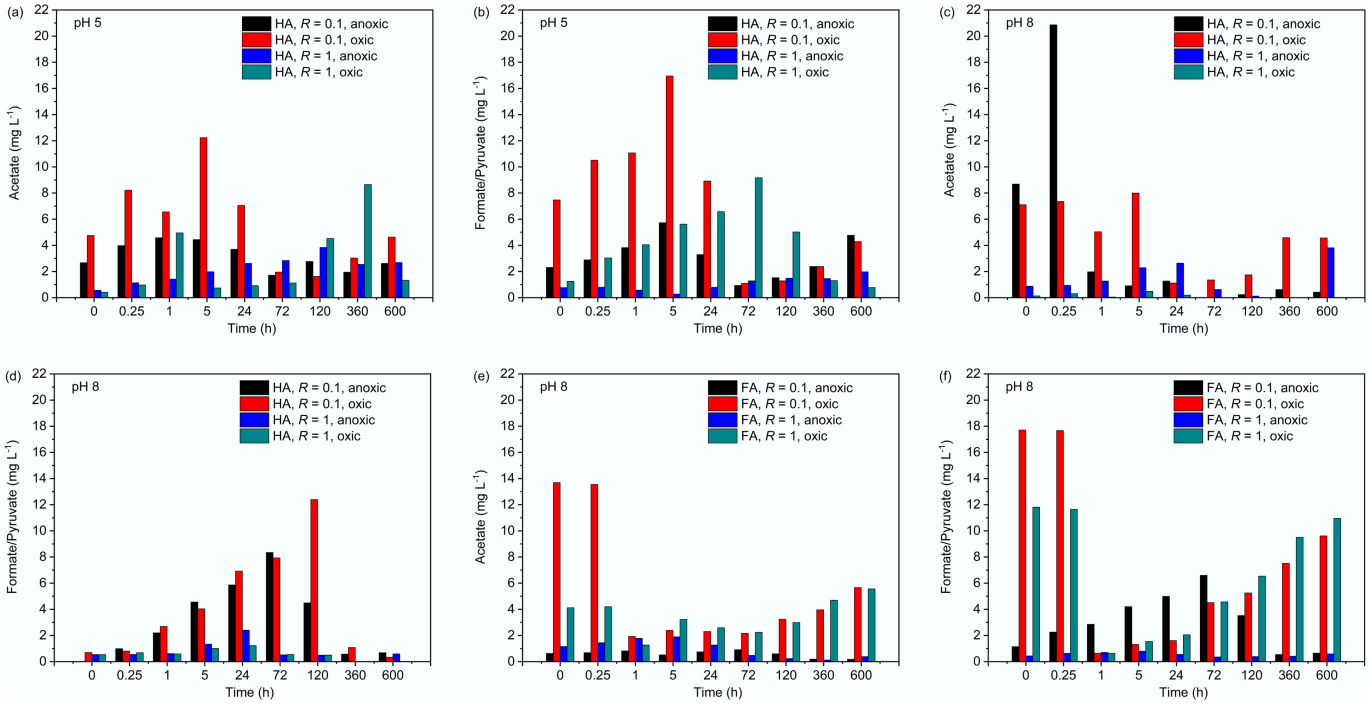


Fig. 3 (**a**), (**c**), (**e**) Concentrations of acetate and (**b**), (**d**), (**f**) formate/pyruvate at different reaction times at pH 5 and 8 with R = 0.1 and 1 under anoxic or oxic conditions. Note: pyruvate had a retention time similar to formate, which makes them indistinguishable by ion chromatography.

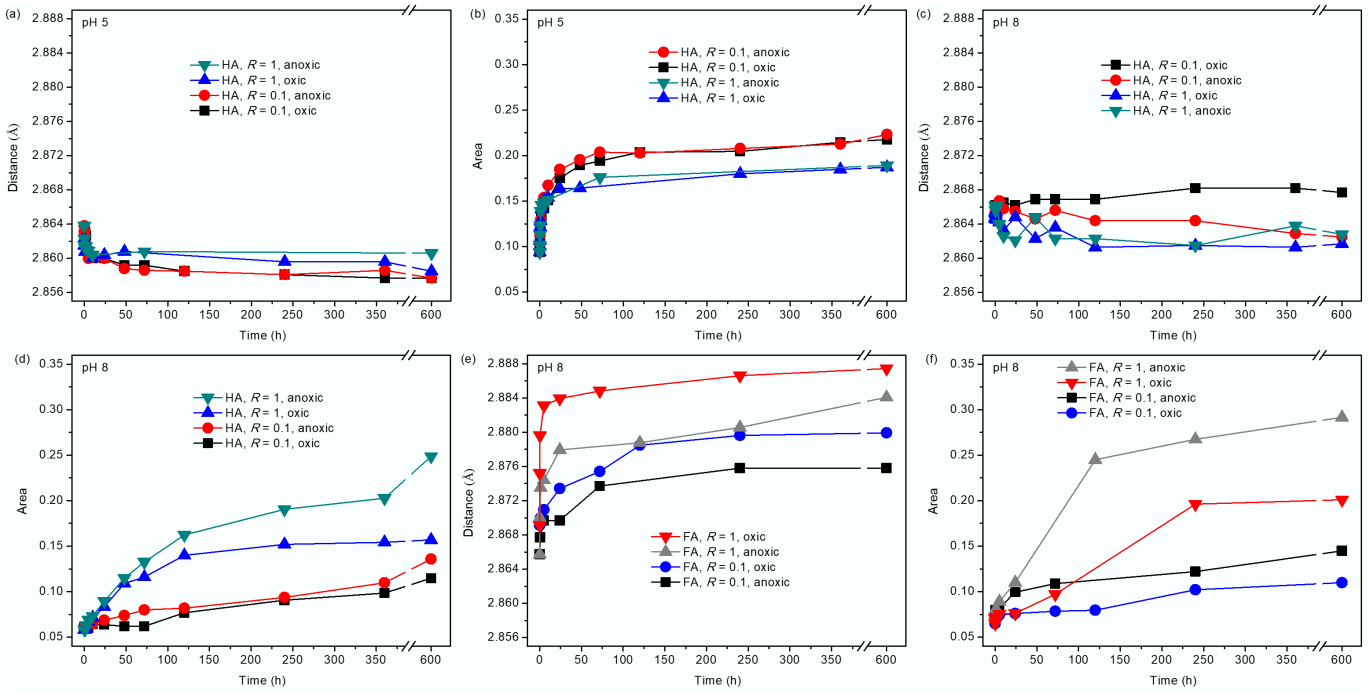


Fig. 4 (**a**), (**c**), (**e**) The Mn_L–Mn_L distance, and (**b**) (**d**), (**f**) the area of the Mn_L–Mn_{IL} peak at ~5.3 Å derived from PDF for δ-MnO_2 reacted with HA or FA at pH 5 and 8 with R = 0.1 and 1. The results for the FA systems under anoxic conditions were reported in Wang et al.[12].

directly degrade HS into partially oxidized HS and CO_2[75,76], therefore suppressing the reduction of δ-MnO_2 by HS and decreasing Mn(II) production. Second, O_2 can oxidize dissolved Mn(II), further lowering $[Mn]_{dis}$. Numerous studies show that dissolved Mn(II) can be oxidized by O_2 into Mn(III) or hausmannite, MnOOH, or δ-MnO_2 via surface-catalyzed mechanisms[77–81]. It was expected that Mn(II) released from HS oxidation in our systems would be oxidized into Mn(III,IV) by O_2, especially at pH 8. Mn(II) oxidation may involve superoxide radical $O_2^{\cdot-}$, which has been proposed as a reactive intermediate in Mn oxidation pathways[82–84]. The two stages of dissolved Mn variations with time at pH 8 with R = 1 in both HA and FA systems (Fig. 1b, c) suggest that Mn(II) release via HS reduction of δ-MnO_2 dominated during the early stage, whereas Mn(II) oxidation by O_2 became dominant at the later stage.

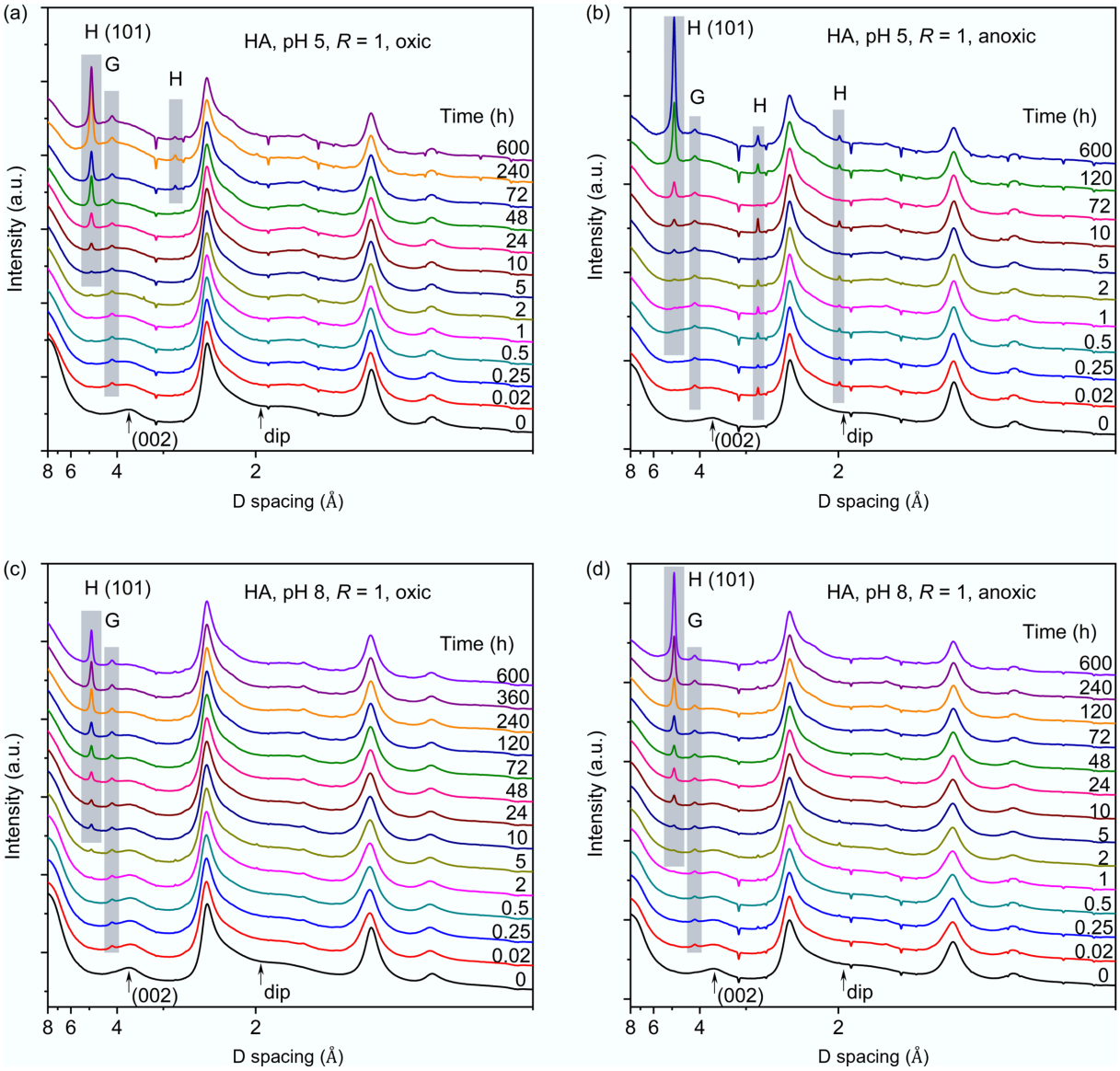


Fig. 5 Synchrotron-based XRD patterns of δ-MnO_2 reacted with humic acid (HA) at (**a**), (**b**) pH 5 and (**c**), (**d**) pH 8 with R = 1. Labels H and G represent hausmannite and groutite, respectively. Note that the inverse peaks in the patterns were caused by subtracted by ceria (CeO_2) standard signal remaining in the empty Kapton capillary.

Although the direct oxidation of HS by O_2 is likely limited, its oxidative reactivity increases significantly at elevated pH due to deprotonation of phenolic and carboxylic groups, which enhances electron donation to reactive oxygen species[76]. Similarly, Mn(II) oxidation by O_2 is strongly pH-dependent[79,80], as hydrolyzed Mn species are more readily oxidized[79], and Mn oxide formation becomes autocatalytic under alkaline conditions[77]. These coupled processes more effectively suppress the production of dissolved Mn at pH 8 than at pH 5. In addition, O_2 may decrease the reactivity of δ-MnO_2 by promoting particle agglomeration and surface passivation associated with enhanced Mn(III) formation from Mn(II)[85]. This effect reduces the reaction of HS with δ-MnO_2, which is the primary pathway generating Mn(II).

Inhibited solid Mn(III) production

The abrupt changes in Mn(II) and Mn(III) from the as-synthesized δ-MnO_2 to the beginning of the reactions suggest a rapid reduction of δ-MnO_2, consistent with the greatest production of LMW organic molecules at the early stage for most of the systems (Fig. 3). These sharp changes may also partly result from the drying process after collecting the first sample when HS was not completely removed by filtration. Subsequent changes in solid Mn(II) and Mn(III) during the reactions are likely correlated with continued interactions between HS and δ-MnO_2, in addition to the drying effects. The molecular differences between HA and FA may partly explain the decrease in Mn(III) accompanied by an increase in Mn(II) observed in all HA systems, but not in all FA systems. Compared with FA, HA contains fewer oxygen-containing functional groups (e.g., carboxylic and phenolic groups)[60], which may contribute to its lower reactivity toward δ-MnO_2. The relatively slower reaction of HA with δ-MnO_2 may allow Mn(III) formed during the initial reduction of Mn(IV) to undergo further transformation, including disproportionation to Mn(II) and Mn(IV), thereby contributing to the decrease in solid-phase Mn(III) and accumulation of Mn(II). The formation of hausmannite (see the section

https://doi.org/10.48130/ebp-0026-0017

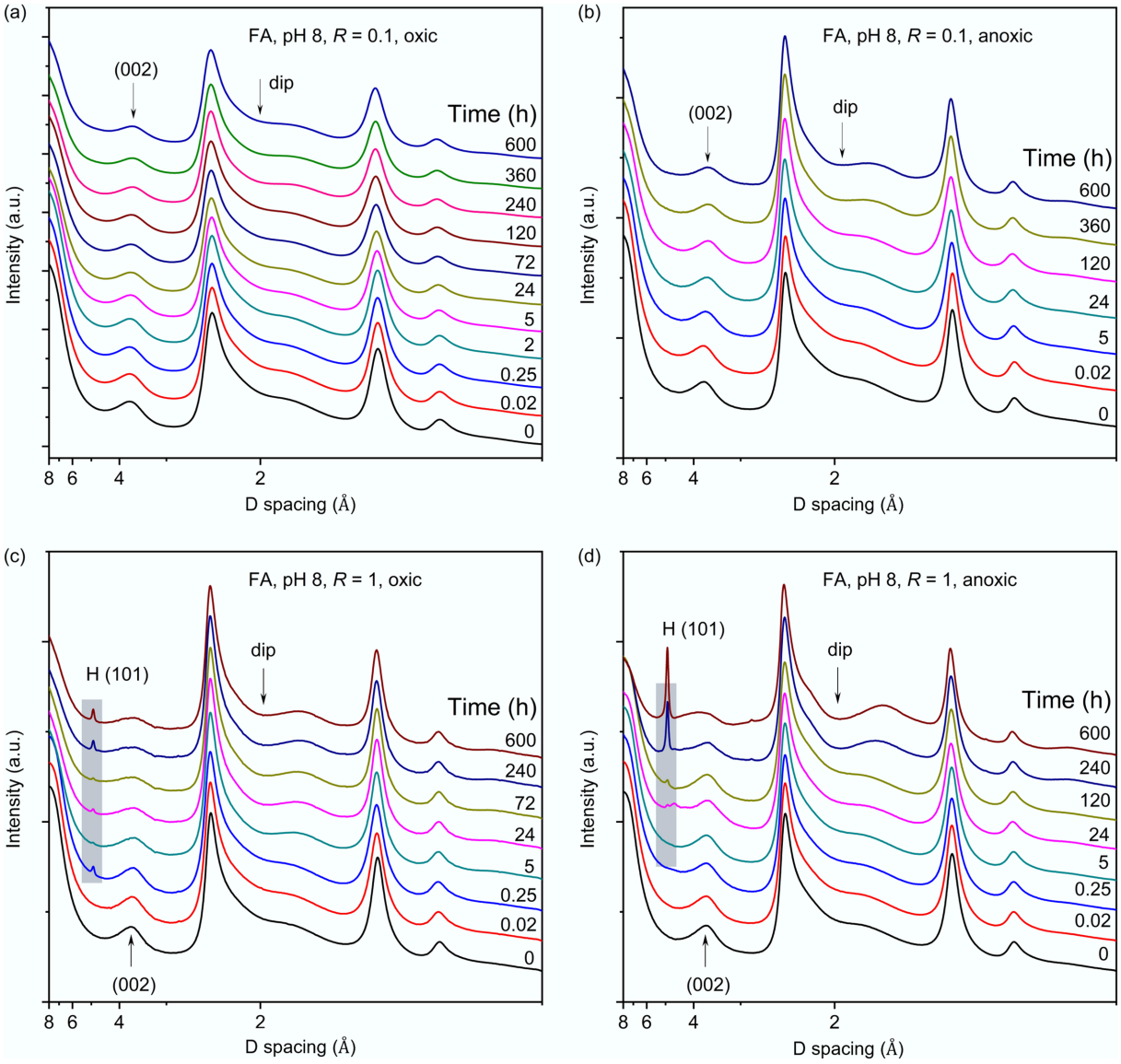


Fig. 6 Synchrotron-based XRD patterns of δ-MnO_2 reacted with FA at (**a**), (**b**) pH 8 with R = 0.1, or (**c**), (**d**) R = 1, under oxic or anoxic conditions. The arrow and the label H indicate the position of the dip and the characteristic peak of hausmannite, respectively. Data for anoxic conditions were adopted from Wang et al.[12].

below) in HA systems provides additional evidence for processes involving Mn(II) and Mn(III), although the observed Mn(II) and Mn(III) changes alone do not establish disproportionation as the sole pathway. Mn(III) may also undergo further reduction by organic matter or become complexed by HA, particularly at alkaline pH[86–91]. In contrast, the faster reaction of FA with δ-MnO_2 may sustain the production and accumulation of Mn(III) while simultaneously promoting Mn(IV) reduction and Mn(II) accumulation. This would result in the concurrent increases in both Mn(III) and Mn(II) observed in the FA systems, even under acidic conditions, consistent with previous observations[12].

Total solid-phase Mn(III) concentrations were lower in the presence of O_2 than under anoxic conditions, with the largest decrease observed in the FA systems at pH 8. The oxidation of FA by O_2 was likely significant, as evidenced by the enhanced production of LMW organic acids. These observations suggest that O_2-promoted oxidation of HS reduced the availability of reactive HS for the reduction of δ-MnO_2, thereby suppressing the generation of Mn(III). In addition, the O_2-enhanced particle aggregation and surface passivation[85] would further inhibit the reaction between HS and Mn(IV) sites in δ-MnO_2. At pH 8, the influence of O_2 was less pronounced in the HA systems than in the FA systems, likely because the slower reaction kinetics of HA allowed the system to approach equilibrium more gradually, thereby diminishing the impact of O_2.

An exception was observed in the FA system at R = 1, where the solid-phase Mn(III) concentration decreased slightly in the presence of O_2. The O_2-promoted degradation of HS was more pronounced in the FA systems than in the HA systems (Fig. 3). At R = 1, the higher FA concentration produced greater amounts of LMW organic compounds, which may have complexed with Mn(III), thereby facilitating the accumulation of Mn(II) in the solid phase. The complexation of Mn(III) by LMW organic ligands has been reported to be enhanced under alkaline conditions[92]. Furthermore, the higher abundance of oxygen-containing functional groups in FA[60] may

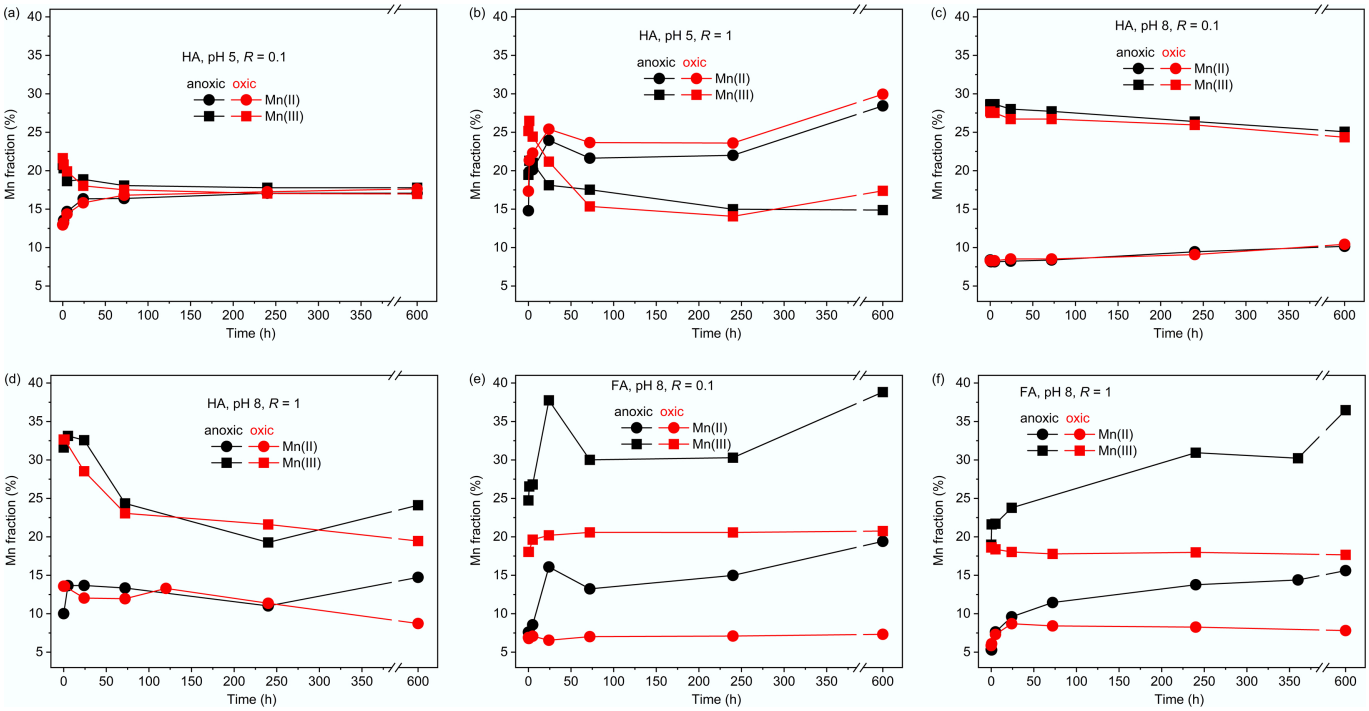


Fig. 7 Mn K-edge XANES LCF-estimated molar fractions of Mn(II) and Mn(III) in δ-MnO_2 reacted with DOM at pH 5 and 8 with (**a**), (**c**), (**e**) R = 0.1 or (**b**), (**d**), (**f**) R = 1 under oxic or anoxic conditions. The molar fraction of Mn(IV) is omitted for clarity of Mn(II) and Mn(III) changes. Refer to Supplementary Fig. S4 for LCF analysis.

have further stabilized Mn(III) through complexation[93]. In contrast, at R = 0.1, the reaction between FA and δ-MnO_2 likely dominated over FA oxidation by O_2. The lower FA concentration and reduced production of LMW organic compounds would have limited Mn(III) complexation, thereby favoring the oxidation of Mn(II) to Mn(III) by O_2 and resulting in higher solid-phase Mn(III) concentrations.

Enhanced Mn(III) accumulation within the layers

The increasing Mn_L–Mn_L distance by PDF analysis should reflect the abundance of Mn(III) in the layers. It should be noted that new phases of hausmannite and groutite (see next section) also have edge-sharing Mn–Mn atomic pairs at distances of 2.88 and 2.82 Å that may also contribute to the change in the Mn_L–Mn_L distance (Fig. 4). However, the number of pairs in unit volume is much lower in hausmannite and groutite than in δ-MnO_2; the contribution to the interatomic distance change from the new phase formation might be insignificant. In addition, the two distances will also cancel out the changes that have been observed between 2.858 and 2.886 Å. Therefore, the PDF-derived Mn_L–Mn_L distance should be positively correlated with the abundance of Mn(III) in the layers.

The higher abundance of layer Mn(III) under oxic conditions in the FA systems and the HA systems at pH 8 with R = 0.1 can be attributed to the oxidation of adsorbed Mn(II) at vacancies or edges by O_2, producing Mn(III) that subsequently incorporates into the δ-MnO_2 layers. As discussed above, the reduction of Mn(IV) by DOM generates Mn(III) through a single-electron transfer[34,94], elongating the Mn_L–Mn_L distance. Even if the generated Mn(III) can be further reduced to Mn(II) through a second single-electron transfer[86,94], Mn(II) adsorbs on the vacant or edge sites, which will be re-oxidized to Mn(III) and will subsequently incorporate into the layers. These processes leave fewer Mn(II,III) species at vacancies (Fig. 4d, f) but enrich the layers in Mn(III) (Fig. 4c, e). Although adsorbed Mn(II) can be oxidized by structural Mn(IV)[51,52], the presence of O_2 enhanced the processes. For example, our previous study showed that O_2 enhances the enrichment of Mn(III) in the layers during the Mn(II)–MnO_2 reactions[51]. The weaker effects of O_2 at pH 5 likely reflect the slower oxidation of Mn(II) by O_2[51,79] and less efficient incorporation of Mn(III) into the layers[51] under more acidic conditions.

An apparent discrepancy exists between the elongated Mn_L–Mn_L distance and the slightly lower solid-phase Mn(III) concentration under oxic conditions in the FA system at R = 1. As discussed above, the slight decrease in solid Mn(III) concentration may result from the complexation of Mn(III) by LMW organic acids and FA. In contrast, the longest Mn_L–Mn_L distance observed under this condition, relative to other conditions, suggests that Mn(III) incorporation into the δ-MnO_2 layers was most strongly favored despite the lower overall solid-phase Mn(III) concentration. The apparent discrepancy can be primarily explained by the decoupling between total solid-phase Mn(III) concentration and Mn(III) enrichment specifically within the δ-MnO_2 layers. O_2 can promote oxidation of Mn(II) and incorporation of the resulting Mn(III) into the δ-MnO_2 structure, consistent with previous observations[51,79]. At the same time, complexation of Mn(III) by LMW organic acids and FA may decrease the amount of Mn(III) detected in the solid phase, particularly by removing Mn(III) associated with vacancy sites. This process could create additional vacant sites that favor subsequent incorporation of Mn(III) into the layers. In addition, O_2 oxidation of FA decreases its reducing capacity, which may favor single-electron transfer during Mn reduction and thereby promote Mn(III) retention within the MnO_2 layers[34].

Suppressed formation of hausmannite and groutite

Hausmannite formation was observed in all HA systems (Fig. 5; Supplementary Fig. S3). Its enhanced formation at higher R at both pH

https://doi.org/10.48130/ebp-0026-0017

values was attributed to greater Mn(II,III) production at higher HA concentrations. Lower pH also promoted hausmannite formation due to favored HA oxidation, as observed in previous studies on humic substances[12,48] and other organic contaminants[4,95,96].

The suppressed formation of hausmannite under oxic conditions may be ascribed to: (1) oxidation of Mn(II) by O_2[79]; (2) HA oxidation by O_2 (Fig. 3)[97,98]; or (3) oxidative transformation of hausmannite back to δ-MnO_2, which is favored under alkaline conditions[55]. Mn(II) oxidation decreases Mn(II) availability for hausmannite formation, and HA oxidation by O_2 decreases HA availability to reduce δ-MnO_2 to Mn(II). The decreased $[Mn]_{dis}$ (Fig. 1) and enhanced production of LMW organic molecules (Figs 2, 3) under oxic conditions suggest that Mn(II) and/or HA oxidation by O_2 is the cause of the suppressed hausmannite formation.

Groutite formation was observed only in the HA systems at R = 1 at both pH 5 and 8 under oxic and anoxic conditions, occurring much earlier (~0.02 h) than hausmannite, likely because groutite is less thermodynamically stable than hausmannite[99] according to the Ostwald step rule[100]. Although groutite is metastable, its enthalpy relative to manganite is small, so transformation to manganite is not favored[101]. Groutite may transform into hausmannite in the presence of Mn(II) at a comparable rate to its formation, resulting in unchanged groutite diffraction peaks (Fig. 5).

The strong reducing capability of FA accounts for the inconsistent formation of hausmannite and groutite at R = 0.1 and 1. At low R, FA may reduce neo-formed hausmannite back to Mn(II), as our previous study showed[12], resulting in higher dissolved Mn at pH 8 than in HA systems. On the other hand, the degradation products of FA, e.g., (poly)phenols, highly unsaturated and phenolic compounds, saturated fatty acids, carbohydrates[28,48], and LMW organics (Fig. 3) such as formate, acetate, oxalate, pyruvate, hydroquinone, formaldehyde, and acetaldehyde[13,14,20,26], can reduce Mn(III) or hausmannite back to Mn(II)[102–104]. The significantly decreased concentrations of acetate and formate/pyruvate after 1 h (Fig. 3e, f) could reflect this effect.

Improved HS degradation

The degradation products of HA and FA included, but were not limited to, pyruvate, formate, and acetate (Fig. 3), consistent with previous studies[13,14,26]. High molecular-weight segments, however, cannot be measured by IC and require characterization by more advanced analytical approaches such as Fourier transform-ion cyclotron resonance mass spectrometry (FT-ICR-MS)[105,106]. Recent FT-ICR-MS studies revealed that polycyclic aromatic hydrocarbons, polyphenols, highly unsaturated carbon and phenolic compounds, aliphatic compounds, and carbohydrates in FA were all involved in reducing δ-MnO_2, which were likely responsible for producing those LMW organic molecules[28,48].

One interesting phenomenon is that the concentrations of LMW organic molecules fluctuated throughout the entire reaction period. As discussed in the previous section, these LMW organic molecules could be oxidized by residual δ-MnO_2 and/or neo-formed hausmannite[107–109]. Although hausmannite generally has a lower oxidation capacity than δ-MnO_2[86,110], its oxidative capability can be enhanced by orders of magnitude in the presence of chelating ligands that complex Mn(III)[86]. In this system, such chelating ligands could include the LMW organic molecules themselves or oxidized HS fragments. By further oxidation, LMW organic molecules may convert to CO_2 that escapes the system or modify the functional groups that change their residence time during IC measurements. For example, oxalate, pyruvate, and citrate can be oxidized to CO_2 by birnessite, manganite, and pyrolusite[107–109], and citrate can be converted to 3-ketoglutarate and acetoacetate by birnessite[108].

Although the concentrations of LMW organic molecules fluctuated throughout the reactions, the presence of O_2 generally enhanced their production. In addition to oxidation by δ-MnO_2, HS can also be oxidized directly by O_2 under oxic conditions[97,111,112], leading to greater production of LMW organic molecules than in anoxic systems. Conversely, O_2 can further oxidize LMW organic molecules to inorganic carbon (CO_2 and carbonate)[113–115]. The competing production and consumption pathways likely contributed to the observed fluctuations in LMW organic molecule concentrations.

For both HS fragments and LMW organic molecules, reactive oxygen species (ROS), such as superoxide ($O_2^{\cdot-}$), singlet oxygen ($O^{\cdot-}$), and hydroxyl (•OH) radicals, may serve as the direct oxidants during O_2-mediated reactions. These ROS have previously been observed during birnessite-catalyzed oxidation of organic and inorganic pollutants under oxic conditions[11,84,116,117]. The generation of ROS is thought to occur through electron transfer from structural Mn(III) to O_2, suggesting that the oxidation rates of HS and LMW organic molecules may depend on Mn(III) abundance. However, such a relationship was not evident in our systems. This lack of correlation likely reflects the complex cycling of Mn(III), which is simultaneously produced through single-electron transfer from HS to Mn(IV) and through Mn(IV)-Mn(II) comproportionation, while being depleted through electron transfer to O_2 during ROS formation and through Mn(III) disproportionation. Together with the direct oxidation of HS by δ-MnO_2[9,12,13,48], these competing pathways obscure any simple dependence of HS oxidation on Mn(III) concentrations.

Another phenomenon commonly observed during organic matter–mineral interactions is OM polymerization, including condensation of (poly)phenols[16,118] and Maillard-type reactions[17,119,120]. For example, DOM extracted from litter or paddy soils exhibited polymerization during interactions with δ-MnO_2[34,121]. In contrast, our recent study of FA interacting with δ-MnO_2 showed little evidence of polymerization[48]. This difference likely arises from compositional variations among DOM sources. The compositional complexity of DOM generally decreases in the order: litter-derived DOM > soil-derived DOM > HA > FA. DOM with greater compositional complexity may be more prone to polymerization due to a wider range of reactive compounds. For example, in litter-derived DOM, highly aromatic and HMW compounds containing oxygen-rich functional groups tend to decompose, whereas low-aromaticity compounds preferentially polymerize[34]. Soil-derived DOM also contains abundant phenolic compounds that can polymerize during interactions with δ-MnO_2[121], which is also manifested by the polymerization of catechol, hydroquinone, and resorcinol[122]. In contrast, aquatic DOM typically contains fewer phenolic compounds[123] and is often dominated by FA[124–126], consistent with the limited polymerization observed in our previous study[48]. Moreover, the isolation and purification of FA as used in the present study involves an alkaline extraction and purification with 0.1 M NaOH[127]. Such alkaline conditions can induce polymerization[128,129], which might have already depleted all the polymerization potential of the organic matter. Such effects could also occur in the HA isolated from soils, as alkaline extraction is also used. However, whether HA underwent polymerization or not during reactions with δ-MnO_2 requires characterization using advanced analytical techniques such as FT-ICR-MS[105,106] and/or fluorescence spectroscopy[130].

Conclusions

This study demonstrates that O_2 affects the coupled redox transformation of δ-MnO_2 and HS rather than simply suppressing Mn reduction. The presence of O_2 redirected Mn–organic matter interactions toward enhanced HS degradation and Mn(III) incorporation into the birnessite structure, while limiting dissolved Mn release, total Mn(III) production, and the formation of secondary Mn minerals such as hausmannite and groutite. These effects were particularly pronounced in FA systems, demonstrating that the influence of O_2 depends on the chemical nature and reactivity of organic matter. Collectively, our results reveal a trade-off in which oxic conditions constrain the structural destabilization and phase transformation of birnessite while promoting continued HS oxidation. This O_2-dependent coupling provides a mechanistic basis for understanding how fluctuations between oxic and anoxic conditions regulate both Mn oxide mineralogy and organic matter stability in soils and sediments. More broadly, our findings demonstrate that redox conditions and organic matter composition jointly control Mn oxide reactivity and transformation pathways, as well as organic C stability, with important implications for coupled Mn and C cycling in natural environments.

Supplementary information

It accompanies this paper at: https://doi.org/10.48130/ebp-0026-0017

Ethical statements

Not applicable.

Author contributions

The authors confirm their contributions to the paper as the following: Peng Yang: methodology, investigation, writing - original draft, writing – review & editing; Qian Wang: conceptualization, methodology, investigation, writing - original draft, writing - review & editing; Mengqiang Zhu: conceptualization, investigation, writing – review & editing, resources, funding acquisition. All authors reviewed the results and approved the final version of the manuscript.

Data availability

The datasets generated and/or analyzed during the current study are available from the corresponding author upon reasonable request.

Acknowledgments

The authors thank Janet Dewey at the Department of Geology and Geophysics, University of Wyoming, for her assistance in ion chromatography measurements. We acknowledge beamline scientists Olaf J. Borkiewicz, Kevin A. Beyer, and Karena W. Chapman at beamline 11-ID-B, Advanced Photon Source, for their assistance in XRD and PDF data collection, and Ryan Davis, Matthew J. Latimer, and Erik J. Nelson for their assistance in XAS data collection at beamline 4-1 at Stanford Synchrotron Radiation Lightsource (SSRL). This research used resources of APS, a US Department of Energy (DOE) Office of Science User Facility operated for the DOE Office of Science by Argonne National Laboratory under Contract No. DE-AC02-06CH11357. Use of SSRL, SLAC National Accelerator Laboratory, was supported by the US DOE, Office of Science, Office of Basic Energy Sciences, under Contract No. DE-AC02-76SF00515.

Funding

This work was primarily supported by the National Science Foundation under DEB-2027284. This work was also supported, in part, by Brookhaven Science Associates, LLC, under Contract No. DE-SC0012704 with the US DOE.

Declarations

Competing interests

The authors declare that they have no known competing financial interests or personal relationships that could have appeared to influence the work reported in this paper.

Author details

[1]Department of Ecosystem Science and Management, University of Wyoming, Laramie, Wyoming 82071, United States; [2]National Synchrotron Light Source-II, Brookhaven National Laboratory, Upton, New York 11973, United States; [3]Carlsbad Environmental Monitoring & Research Center, New Mexico State University, Carlsbad, New Mexico 88220, United States; [4]Department of Geological, Environmental, and Planetary Sciences, University of Maryland, College Park, Maryland 20742, United States

References

[1] Post JE. 1999. Manganese oxide minerals: crystal structures and economic and environmental significance. *Proceedings of the National Academy of Sciences of the United States of America* 96:3447–3454

[2] Lafferty BJ, Ginder-Vogel M, Sparks DL. 2010. Arsenite oxidation by a poorly crystalline manganese-oxide 1. Stirred-flow experiments. *Environmental Science & Technology* 44:8460–8466

[3] Landrot G, Ginder-Vogel M, Livi K, Fitts JP, Sparks DL. 2012. Chromium(III) oxidation by three poorly-crystalline manganese(IV) oxides. 1. Chromium(III)-oxidizing capacity. *Environmental Science & Technology* 46:11594–11600

[4] Remucal CK, Ginder-Vogel M. 2014. A critical review of the reactivity of manganese oxides with organic contaminants. *Environmental Science: Processes & Impacts* 16:1247–1266

[5] Li F, Yin H, Zhu T, Zhuang W. 2024. Understanding the role of manganese oxides in retaining harmful metals: insights into oxidation and adsorption mechanisms at microstructure level. *Eco-Environment & Health* 3:89–106

[6] Shi M, Li Q, Wang Q, Yan X, Li B, et al. 2024. A review on the transformation of birnessite in the environment: implication for the stabilization of heavy metals. *Journal of Environmental Sciences* 139:496–515

[7] Wen K, Yang Y, Li S, Xi J, Yi R, et al. 2026. Crystallinity-dependent transformation of layered manganese oxides: implications for the mineral diversity of manganese oxides in nature. *National Science Review* 13:nwag392

[8] Yang S, Shobnam N, Sun Y, Löffler FE, Im J. 2024. The relative contributions of Mn(III) and Mn(IV) in manganese dioxide polymorphs to bisphenol A degradation. *Journal of Hazardous Materials* 461:132596

[9] Wang Q, Yang P, Zhu M. 2019. Effects of metal cations on coupled birnessite structural transformation and natural organic matter adsorption and oxidation. *Geochimica et Cosmochimica Acta* 250:292–310

[10] Li H, Atkins B, Williams S, Yin H, Reinhart B, et al. 2024. Sorption and oxidative degradation of small organic molecules on

https://doi.org/10.48130/ebp-0026-0017

Mn-oxides—effects of pH and mineral structures. *ACS Earth and Space Chemistry* 8:2067–2077
[11] Zhou Y, Guo C, Deng Y, Jiang Y, Yin M, et al. 2025. Birnessite enhanced Cr(III) oxidation during subsurface geochemical processes: role of Mn(III)-induced nonphotochemical reactive oxygen species. *Environmental Pollution* 366:125436
[12] Wang Q, Yang P, Zhu M. 2018. Structural transformation of birnessite by fulvic acid under anoxic conditions. *Environmental Science & Technology* 52:1844–1853
[13] Ma D, Wu J, Yang P, Zhu M. 2020. Coupled manganese redox cycling and organic carbon degradation on mineral surfaces. *Environmental Science & Technology* 54:8801–8810
[14] Allard S, Gutierrez L, Fontaine C, Croué JP, Gallard H. 2017. Organic matter interactions with natural manganese oxide and synthetic birnessite. *Science of the Total Environment* 583:487–495
[15] Li H, Santos F, Butler K, Herndon E. 2021. A critical review on the multiple roles of manganese in stabilizing and destabilizing soil organic matter. *Environmental Science & Technology* 55:12136–12152
[16] Shindo H, Huang PM. 1982. Role of Mn(IV) oxide in abiotic formation of humic substances in the environment. *Nature* 298:363–365
[17] Jokic A, Frenkel AI, Vairavamurthy MA, Huang PM. 2001. Birnessite catalysis of the Maillard reaction: its significance in natural humification. *Geophysical Research Letters* 28:3899–3902
[18] Johnson K, Purvis G, Lopez-Capel E, Peacock C, Gray N, et al. 2015. Towards a mechanistic understanding of carbon stabilization in manganese oxides. *Nature Communications* 6:7628
[19] Moore OW, Curti L, Woulds C, Bradley JA, Babakhani P, et al. 2023. Long-term organic carbon preservation enhanced by iron and manganese. *Nature* 621:312–317
[20] Sunda WG, Kieber DJ. 1994. Oxidation of humic substances by manganese oxides yields low-molecular-weight organic substrates. *Nature* 367:62–64
[21] Sunda WG, Huntsman SA, Harvey GR. 1983. Photoreduction of manganese oxides in seawater and its geochemical and biological implications. *Nature* 301:234–236
[22] Waite TD, Wrigley IC, Szymczak R. 1988. Photoassisted dissolution of a colloidal manganese oxide in the presence of fulvic acid. *Environmental Science & Technology* 22:778–785
[23] Jin C, Li Z, Hursthouse AS, Ding X, Zhou M, et al. 2023. Manganese oxides mediated dissolve organic matter compositional changes in lake sediment and cadmium binding characteristics. *Ecotoxicology and Environmental Safety* 256:114916
[24] Stuckey JW, Goodwin C, Wang J, Kaplan LA, Vidal-Esquivel P, et al. 2018. Impacts of hydrous manganese oxide on the retention and lability of dissolved organic matter. *Geochemical Transactions* 19:6
[25] Ding Z, Hu S, Zhu L, Xiao J, Ye Q, et al. 2024. Multiple effects of iron oxides on the adsorption and oxidation of dissolved organic matter by manganese oxides. *Geochimica et Cosmochimica Acta* 384:213–227
[26] Chorover J, Amistadi MK. 2001. Reaction of forest floor organic matter at goethite, birnessite and smectite surfaces. *Geochimica et Cosmochimica Acta* 65:95–109
[27] Liu H, Li Y, Huangfu Z, Lu Q, Yang B, et al. 2024. Structure and molecular-level transformation for oxidation of effluent organic matters by manganese oxides. *Water Research* 262:122082
[28] Zhang X, Zhou X, Ma Y, Zhang W, Zhang R, et al. 2025. Contrasting reaction of dissolved organic matter with birnessite induced by humic and fulvic acids in flooded paddy soil. *Sustainability* 17:7203
[29] Berg B, Davey MP, De Marco A, Emmett B, Faituri M, et al. 2010. Factors influencing limit values for pine needle litter decomposition: a synthesis for boreal and temperate pine forest systems. *Biogeochemistry* 100:57–73
[30] Keiluweit M, Nico P, Harmon ME, Mao J, Pett-Ridge J, et al. 2015. Long-term litter decomposition controlled by manganese redox cycling. *Proceedings of the National Academy of Sciences of the United States of America* 112:E5253–E5260
[31] Berg B, Steffen KT, McClaugherty C. 2007. Litter decomposition rate is dependent on litter Mn concentrations. *Biogeochemistry* 82:29–39
[32] Berg B, Erhagen B, Johansson MB, Nilsson M, Stendahl J, et al. 2015. Manganese in the litter fall-forest floor continuum of boreal and temperate pine and spruce forest ecosystems – a review. *Forest Ecology and Management* 358:248–260
[33] Xiao KQ, Zhao Y, Liang C, Zhao M, Moore OW, et al. 2023. Introducing the soil mineral carbon pump. *Nature Reviews Earth & Environment* 4:135–136
[34] Jiang F, Su H, Fu QL, Yang Z, Wang X, et al. 2025. Manganese oxides drive divergent fates of litter-derived DOM via pH-regulated oxidative decomposition and polymerization. *Environmental Science & Technology* 59:25251–25264
[35] Marhaba TF, Pu Y. 2000. Rapid delineation of humic and non-humic organic matter fractions in water. *Journal of Hazardous Materials* 73:221–234
[36] Estes ER, Andeer PF, Nordlund D, Wankel SD, Hansel CM. 2017. Biogenic manganese oxides as reservoirs of organic carbon and proteins in terrestrial and marine environments. *Geobiology* 15:158–172
[37] Huang X, Dou Y, Yang B, Ding Y. 2025. Immobilization and release behaviors of uranium mediated by the redox processes between manganese oxides and dissolved organic matter: effects of pH and goethite. *Journal of Hazardous Materials* 490:137860
[38] Huang X, Yang B, Dou Y, Ding Y. 2025. Coupled transformations of manganese and dissolved organic matter molecules during iron (oxyhydr)oxide-catalyzed oxidation of Mn(II). *Journal of Environmental Sciences* 155:538–551
[39] Swenson JT, Ginder-Vogel M, Remucal CK. 2024. Influence of divalent cation inhibition and dissolved organic matter enhancement on phenol oxidation kinetics by manganese oxides. *Environmental Science & Technology* 58:2479–2489
[40] Li Q, Hausladen DM. 2025. Impact of organic carbon-Mn oxide interactions on colloid stability and contaminant metals in aquatic environments. *Water Research* 280:123445
[41] Qi H, Zhang A, Du Z, Wu J, Chen X, et al. 2021. δ-MnO_2 changed the structure of humic-like acid during co-composting of chicken manure and rice straw. *Waste Management* 128:16–24
[42] Zhang Y, Yue D, Wang X, Song W. 2019. Mechanism of oxidation and catalysis of organic matter abiotic humification in the presence of MnO_2. *Journal of Environmental Sciences* 77:167–173
[43] Shi Y, Wang Z, Jia H, Li C. 2024. Insights into the transformation of dissolved organic matter and carbon preservation on a MnO_2 surface: effect of molecular weight of dissolved organic matter. *Science of the Total Environment* 945:174022
[44] Banerjee D, Nesbitt HW. 1999. XPS study of reductive dissolution of birnessite by oxalate: rates and mechanistic aspects of dissolution and redox processes. *Geochimica et Cosmochimica Acta* 63:3025–3038
[45] Banerjee D, Nesbitt HW. 2001. XPS study of dissolution of birnessite by humate with constraints on reaction mechanism. *Geochimica et Cosmochimica Acta* 65:1703–1714
[46] Shaikh N, Taujale S, Zhang H, Artyushkova K, Ali AMS, et al. 2016. Spectroscopic investigation of interfacial interaction of manganese oxide with triclosan, aniline, and phenol. *Environmental Science & Technology* 50:10978–10987
[47] Shaikh N, Zhang H, Rasamani K, Artyushkova K, Ali AMS, et al. 2018. Reaction of bisphenol A with synthetic and commercial $MnO_{x(s)}$: spectroscopic and kinetic study. *Environmental Science: Processes & Impacts* 20:1046–1055
[48] Zhang J, McKenna AM, Zhu M. 2021. Macromolecular characterization of compound selectivity for oxidation and oxidative alterations of dissolved organic matter by manganese oxide. *Environmental Science & Technology* 55:7741–7751
[49] Zou J, Huang J, Yue D, Zhang H. 2020. Roles of oxygen and Mn (IV) oxide in abiotic formation of humic substances by oxidative polymerization of polyphenol and amino acid. *Chemical Engineering Journal* 393:124734
[50] Wang Z, Jia H, Zhao H, Zhang R, Zhang C, et al. 2022. Oxygen limitation accelerates regeneration of active sites on a MnO_2

surface: promoting transformation of organic matter and carbon preservation. *Environmental Science & Technology* 56:9806–9815

[51] Yang P, Lee S, Post JE, Xu H, Wang Q, et al. 2018. Trivalent manganese on vacancies triggers rapid transformation of layered to tunneled manganese oxides (TMOs): implications for occurrence of TMOs in low-temperature environment. *Geochimica et Cosmochimica Acta* 240:173–190

[52] Lefkowitz JP, Rouff AA, Elzinga EJ. 2013. Influence of pH on the reductive transformation of birnessite by aqueous Mn(II). *Environmental Science & Technology* 47:10364–10371

[53] Mandernack KW, Post J, Tebo BM. 1995. Manganese mineral formation by bacterial spores of the marine *Bacillus*, strain SG-1: evidence for the direct oxidation of Mn(II) to Mn(IV). *Geochimica et Cosmochimica Acta* 59:4393–4408

[54] Tu S, Racz GJ, Goh TB. 1994. Transformations of synthetic birnessite as affected by pH and manganese concentration. *Clays and Clay Minerals* 42:321–330

[55] Cornell RM, Giovanoli R. 1988. Transformation of hausmannite into birnessite in alkaline media. *Clays and Clay Minerals* 36:249–257

[56] Hem JD, Lind CJ. 1983. Nonequilibrium models for predicting forms of precipitated manganese oxides. *Geochimica et Cosmochimica Acta* 47:2037–2046

[57] Leenheer JA, Wershaw RL, Reddy MM. 1995. Strong-acid, carboxyl-group structures in fulvic acid from the Suwannee River, Georgia. 1. Minor structures. *Environmental Science & Technology* 29:393–398

[58] Leenheer JA, Wershaw RL, Reddy MM. 1995. Strong-acid, carboxyl-group structures in fulvic acid from the Suwannee River, Georgia. 2. Major structures. *Environmental Science & Technology* 29:399–405

[59] Perminova IV, Frimmel FH, Kudryavtsev AV, Kulikova NA, Abbt-Braun G, et al. 2003. Molecular weight characteristics of humic substances from different environments as determined by size exclusion chromatography and their statistical evaluation. *Environmental Science & Technology* 37:2477–2485

[60] Gaffney JS, Marley NA, Clark SB. 1996. *Humic and Fulvic Acids: Isolation, Structure, and Environmental Role*. USA: American Chemical Society. doi:10.1021/bk-1996-0651

[61] He Z, Olk DC, Cade-Menun BJ. 2011. Forms and lability of phosphorus in humic acid fractions of Hord silt loam soil. *Soil Science Society of America Journal* 75:1712–1722

[62] Kuwatsuka S, Watanabe A, Itoh K, Arai S. 1992. Comparison of two methods of preparation of humic and fulvic acids, IHSS method and NAGOYA method. *Soil Science and Plant Nutrition* 38:23–30

[63] Weltje L, den Hollander W, Wolterbeek HT. 2003. Adsorption of metals to membrane filters in view of their speciation in nutrient solution. *Environmental Toxicology and Chemistry* 22:265–271

[64] Hayashita T, Takagi M. 1985. Sorption and permeation behaviour of metal thiocyanate complexes on cellulose acetate polymers. *Talanta* 32:399–405

[65] Hammersley AP. 2016. *FIT2D*: a multi-purpose data reduction, analysis and visualization program. *Journal of Applied Crystallography* 49:646–652

[66] Qiu X, Thompson JW, Billinge SJL. 2004. *PDFgetX2*: a GUI-driven program to obtain the pair distribution function from X-ray powder diffraction data. *Journal of Applied Crystallography* 37:678

[67] Terban MW, Billinge SJL. 2022. Structural analysis of molecular materials using the pair distribution function. *Chemical Reviews* 122:1208–1272

[68] Ravel B, Newville M. 2005. *ATHENA*, *ARTEMIS*, *HEPHAESTUS*: data analysis for X-ray absorption spectroscopy using *IFEFFIT*. *Journal of Synchrotron Radiation* 12:537–541

[69] Manceau A, Marcus MA, Grangeon S. 2012. Determination of Mn valence states in mixed-valent manganates by XANES spectroscopy. *American Mineralogist* 97:816–827

[70] De Haan H, Werlemark G, De Boer T. 1983. Effect of pH on molecular weight and size of fulvic acids in drainage water from peaty grassland in NW Netherlands. *Plant and Soil* 75:63–73

[71] Peuravuori J, Pihlaja K. 1997. Molecular size distribution and spectroscopic properties of aquatic humic substances. *Analytica Chimica Acta* 337:133–149

[72] Flynn ED, Catalano JG. 2019. Reductive transformations of layered manganese oxides by small organic acids and the fate of trace metals. *Geochimica et Cosmochimica Acta* 250:149–172

[73] Villalobos M, Lanson B, Manceau A, Toner B, Sposito G. 2006. Structural model for the biogenic Mn oxide produced by *Pseudomonas putida*. *American Mineralogist* 91:489–502

[74] Drits VA, Lanson B, Gaillot AC. 2007. Birnessite polytype systematics and identification by powder X-ray diffraction. *American Mineralogist* 92:771–788

[75] Bastviken D, Persson L, Odham G, Tranvik L. 2004. Degradation of dissolved organic matter in oxic and anoxic lake water. *Limnology and Oceanography* 49:109–116

[76] Roginsky V, Barsukova T. 2000. Kinetics of oxidation of hydroquinones by molecular oxygen. Effect of superoxide dismutase. *Journal of the Chemical Society, Perkin Transactions 2* 29:1575–1582

[77] Hu S, Zheng L, Zhang H, Chen G, Yang Y, et al. 2023. Hematite-mediated Mn(II) abiotic oxidation under oxic conditions: pH effect and mineralization. *Journal of Colloid and Interface Science* 636:267–278

[78] Hem JD. 1981. Rates of manganese oxidation in aqueous systems. *Geochimica et Cosmochimica Acta* 45:1369–1374

[79] Morgan JJ. 2005. Kinetics of reaction between O_2 and Mn(II) species in aqueous solutions. *Geochimica et Cosmochimica Acta* 69:35–48

[80] Kessick MA, Morgan JJ. 1975. Mechanism of autoxidation of manganese in aqueous solution. *Environmental Science & Technology* 9:157–159

[81] Bricker O. 1965. Some stability relations in the system Mn-O_2-H_2O at 25° and one atmosphere total pressure. *American Mineralogist* 50:1296–1354

[82] Li Q, Huang X, Su G, Zheng M, Huang C, et al. 2018. The regular/persistent free radicals and associated reaction mechanism for the degradation of 1, 2, 4-trichlorobenzene over different MnO_2 polymorphs. *Environmental Science & Technology* 52:13351–13360

[83] Liu J, Chen Q, Yang Y, Wei H, Laipan M, et al. 2022. Coupled redox cycling of Fe and Mn in the environment: the complex interplay of solution species with Fe- and Mn-(oxyhydr)oxide crystallization and transformation. *Earth-Science Reviews* 232:104105

[84] Wang Z, Jia H, Liu Z, Peng Z, Dai Y, et al. 2021. Greatly enhanced oxidative activity of δ-MnO_2 to degrade organic pollutants driven by dominantly exposed {–111} facets. *Journal of Hazardous Materials* 413:125285

[85] Hu E, Pan S, Zhang W, Zhao X, Liao B, et al. 2019. Impact of dissolved O_2 on phenol oxidation by δ-MnO_2. *Environmental Science: Processes & Impacts* 21:2118–2127

[86] Lu X, Wang X, He H, Liu Q, Li J, et al. 2025. Bisphenol A degradation by manganese oxides at circumneutral pH: quantitative evaluation of dissolved Mn(III) species with pyrophosphate. *Journal of Hazardous Materials* 486:137013

[87] Sun S, Wang Y, Zhou L, Wang X, Kang C. 2022. Enhanced degradation mechanism of tetracycline by MnO_2 with the presence of organic acids. *Chemosphere* 286:131606

[88] Hu E, Zhang Y, Wu S, Wu J, Liang L, et al. 2017. Role of dissolved Mn(III) in transformation of organic contaminants: non-oxidative versus oxidative mechanisms. *Water Research* 111:234–243

[89] Nico PS, Zasoski RJ. 2001. Mn(III) center availability as a rate controlling factor in the oxidation of phenol and sulfide on δ-MnO_2. *Environmental Science & Technology* 35:3338–3343

[90] Huang J, Zhong S, Dai Y, Liu CC, Zhang H. 2018. Effect of MnO_2 phase structure on the oxidative reactivity toward bisphenol A degradation. *Environmental Science & Technology* 52:11309–11318

[91] Li Q, Xie L, Jiang Y, Fortner JD, Yu K, et al. 2019. Formation and stability of NOM-Mn(III) colloids in aquatic environments. *Water Research* 149:190–201

[92] Klewicki JK, Morgan JJ. 1998. Kinetic behavior of Mn(III) complexes of pyrophosphate, EDTA, and citrate. *Environmental Science & Technology* 32:2916–2922

[93] Oldham VE, Mucci A, Tebo BM, Luther GW III. 2017. Soluble Mn(III)–L complexes are abundant in oxygenated waters and stabilized by humic ligands. *Geochimica et Cosmochimica Acta* 199:238–246
[94] Luther GW, Thibault de Chanvalon A, Oldham VE, Estes ER, Tebo BM, et al. 2018. Reduction of manganese oxides: thermodynamic, kinetic and mechanistic considerations for one- versus two-electron transfer steps. *Aquatic Geochemistry* 24:257–277
[95] Wang L, Cheng H. 2015. Birnessite (δ-MnO_2) mediated degradation of organoarsenic feed additive p-arsanilic acid. *Environmental Science & Technology* 49:3473–3481
[96] Lin K, Liu W, Gan J. 2009. Oxidative removal of bisphenol A by manganese dioxide: efficacy, products, and pathways. *Environmental Science & Technology* 43:3860–3864
[97] Page SE, Sander M, Arnold WA, McNeill K. 2012. Hydroxyl radical formation upon oxidation of reduced humic acids by oxygen in the dark. *Environmental Science & Technology* 46:1590–1597
[98] Zeng Q, Wang X, Liu X, Huang L, Hu J, et al. 2020. Mutual interactions between reduced Fe-bearing clay minerals and humic acids under dark, oxygenated conditions: hydroxyl radical generation and humic acid transformation. *Environmental Science & Technology* 54:15013–15023
[99] Inoué S, Yasuhara A, Ai H, Hochella MF Jr, Murayama M. 2019. Mn(II) oxidation catalyzed by nanohematite surfaces and manganite/hausmannite core-shell nanowire formation by self-catalytic reaction. *Geochimica et Cosmochimica Acta* 258:79–96
[100] Van Santen RA. 1984. The Ostwald step rule. *The Journal of Physical Chemistry* 88:5768–5769
[101] Fritsch S, Post JE, Navrotsky A. 1997. Energetics of low-temperature polymorphs of manganese dioxide and oxyhydroxide. *Geochimica et Cosmochimica Acta* 61:2613–2616
[102] Adamčíková L, Krížová A, Valent I. 1993. Kinetics of the manganese(III)-oxalate reaction in acidic sulphate media. *Transition Metal Chemistry* 18:218–220
[103] Barek J, Berka A, Hladíková A. 1979. Oxidation of organic substances with compounds of trivalent manganese: XIII. Oxidation of pyruvic acid with manganese(III) sulfate in a medium of sulfuric acid and with hexaquomanganese(III) ions in noncomplexing medium of perchloric acid. *Microchemical Journal* 24:316–322
[104] Kung KH, McBride MB. 1988. Electron transfer processes between hydroquinone and hausmannite (Mn_3O_4). *Clays and Clay Minerals* 36:297–302
[105] Marshall AG, Hendrickson CL, Jackson GS. 1998. Fourier transform ion cyclotron resonance mass spectrometry: a primer. *Mass Spectrometry Reviews* 17:1–35
[106] Kim S, Kramer RW, Hatcher PG. 2003. Graphical method for analysis of ultrahigh-resolution broadband mass spectra of natural organic matter, the van Krevelen diagram. *Analytical Chemistry* 75:5336–5344
[107] Stone AT. 1987. Microbial metabolites and the reductive dissolution of manganese oxides: oxalate and pyruvate. *Geochimica et Cosmochimica Acta* 51:919–925
[108] Wang Y, Stone AT. 2006. The citric acid–$Mn^{III, IV}$ O_2(birnessite) reaction. Electron transfer, complex formation, and autocatalytic feedback. *Geochimica et Cosmochimica Acta* 70:4463–4476
[109] Xyla AG, Sulzberger B, Luther GW, III, Hering JG, Van Cappellen P, et al. 1992. Reductive dissolution of manganese(III, IV) (hydr)oxides by oxalate: the effect of pH and light. *Langmuir* 8:95–103
[110] Feng XH, Zhai LM, Tan WF, Liu F, He JZ. 2007. Adsorption and redox reactions of heavy metals on synthesized Mn oxide minerals. *Environmental Pollution* 147:366–373
[111] Hulthe G, Hulth S, Hall POJ. 1998. Effect of oxygen on degradation rate of refractory and labile organic matter in continental margin sediments. *Geochimica et Cosmochimica Acta* 62:1319–1328
[112] García M, Collado S, Oulego P, Díaz M. 2020. The wet oxidation of aqueous humic acids. *Journal of Hazardous Materials* 396:122402
[113] Jefferson WA, Hu C, Liu H, Qu J. 2015. Reaction of aqueous Cu–Citrate with MnO_2 birnessite: characterization of Mn dissolution, oxidation products and surface interactions. *Chemosphere* 119:1–7
[114] Mang C, Li G, Zhang X, Luo J, Jiang H, et al. 2022. Preparation of porous birnessite nanospheres derived from pyrolusite–pyrite acid leach solution and their evaluation as a catalyst for formaldehyde decomposition. *ACS Sustainable Chemistry & Engineering* 10:6538–6548
[115] Ritschel T, Totsche KU. 2023. Reductive transformation of birnessite by low-molecular-weight organic acids. *Chemosphere* 325:138414
[116] Chen J, Han Z, Wang C, Liu H, Chen T, et al. 2025. Oxidative degradation of formaldehyde by birnessite: synergistic interaction of Mn(III) and oxygen vacancies. *Applied Surface Science* 681:161526
[117] Zhang S, Lv J, Han R, Wang Z, Christie P, et al. 2021. Sustained production of superoxide radicals by manganese oxides under ambient dark conditions. *Water Research* 196:117034
[118] Stone AT. 1987. Reductive dissolution of manganese(III/Iv) oxides by substituted phenols. *Environmental Science & Technology* 21:979–988
[119] Jokic A, Wang MC, Liu C, Frenkel AI, Huang PM. 2004. Integration of the polyphenol and Maillard reactions into a unified abiotic pathway for humification in nature: the role of δ-MnO_2. *Organic Geochemistry* 35:747–762
[120] Chang RR, Wang SL, Liu YT, Chan YT, Hung JT, et al. 2016. Interactions of the products of oxidative polymerization of hydroquinone as catalyzed by birnessite with Fe (hydr)oxides – an implication of the reactive pathway for humic substance formation. *RSC Advances* 6:20750–20760
[121] Ding Z, Ding Y, Liu F, Yang J, Li R, et al. 2022. Coupled sorption and oxidation of soil dissolved organic matter on manganese oxides: nano/sub-nanoscale distribution and molecular transformation. *Environmental Science & Technology* 56:2783–2793
[122] Ling X, Chen R, Dong B, Xu Z. 2026. Unraveling the mechanisms of abiotic humification mediated by manganese dioxide polymorphs: the dual roles of oxygen vacancies and surface Mn(III). *Chemical Engineering Journal* 535:175496
[123] Judd KE, Crump BC, Kling GW. 2007. Bacterial responses in activity and community composition to photo-oxidation of dissolved organic matter from soil and surface waters. *Aquatic Sciences* 69:96–107
[124] Tsuda K, Mori H, Asakawa D, Yanagi Y, Kodama H, et al. 2010. Characterization and grouping of aquatic fulvic acids isolated from clearwater rivers and lakes in Japan. *Water Research* 44:3837–3846
[125] Ma H, Allen HE, Yin Y. 2001. Characterization of isolated fractions of dissolved organic matter from natural waters and a wastewater effluent. *Water Research* 35:985–996
[126] Malcolm RL, Aiken GR, Bowles EG, Malcolm JD. 1989. Isolation of Fulvic and Humic Acids from the Suwannee River. In *Humic substances in the Suwannee River, Georgia; interactions, properties, and proposed structures*, eds. Averett RC, Leenheer JA, McKnight DM, Thorn KA. Report No. 87-557. Denver: U.S. Geological Survey. pp. 23–36 doi: 10.3133/ofr87557
[127] Thurman EM, Malcolm RL. 1981. Preparative isolation of aquatic humic substances. *Environmental Science & Technology* 15:463–466
[128] Atkins B, Kalu S, Li H. 2025. Characterizing the effect of pH and molecular structure on the reactions of catechol and hydroquinone with birnessite. *Environmental Science & Technology* 59:27279–27290
[129] Lehmann J, Kleber M. 2015. The contentious nature of soil organic matter. *Nature* 528:60–68
[130] Wu P, Fu QL, Zhu XD, Liu C, Dang F, et al. 2020. Contrasting impacts of pH on the abiotic transformation of hydrochar-derived dissolved organic matter mediated by δ-MnO_2. *Geoderma* 378:114627

Copyright: © 2026 by the author(s). Published by Maximum Academic Press, Fayetteville, GA. This article is an open access article distributed under Creative Commons Attribution License (CC BY 4.0), visit https://creativecommons.org/licenses/by/4.0/.